Archives of Biochemistry and Biophysics 681 (2020) 108265

Contents lists available at ScienceDirect

Archives of Biochemistry and Biophysics

journal homepage: www.elsevier.com/locate/yabbi

Interaction of Sp1 and *APP* promoter elucidates a mechanism for Pb^{2+} caused neurodegeneration

Qi Gao[a], Ziwen Dai[b,e], Shiqing Zhang[c], Yuqiang Fang[d], Ken Kin Lam Yung[c,**], Pik Kwan Lo[b,e,***], King Wai Chiu Lai[a,*]

[a] Department of Biomedical Engineering, Centre for Robotics and Automation, City University of Hong Kong, Kowloon, Hong Kong SAR, China
[b] Department of Chemistry, City University of Hong Kong, Kowloon, Hong Kong SAR, China
[c] Department of Biology, Hong Kong Baptist University, Kowloon, Hong Kong SAR, China
[d] School of Mechanical Science and Engineering, Jilin University, Changchun, 130025, China
[e] Key Laboratory of Biochip Technology, Biotech and Health Centre, Shenzhen Research Institute of City University of Hong Kong, Shenzhen, 518057, China

ARTICLE INFO

Keywords:
Atomic force microscope
Zinc finger
Amyloid precursor protein

ABSTRACT

A ubiquitously expressed transcription factor, specificity protein 1 (Sp1), interacts with the amyloid precursor protein (*APP*) promoter and likely mediates APP expression. Promoter-interaction strengths variably regulate the level of APP expression. Here, we examined the interactions of finger 3 of Sp1 (Sp1–f3) with a DNA fragment containing the *APP* promoter in different ionic solutions using atomic force microscope (AFM) spectroscopy. Sp1–f3 molecules immobilized on an Si substrate were bound to the *APP* promoter, which was linked to the AFM tips via covalent bonds. The interactions were strongly influenced by Pb^{2+}, considering that substituting Zn^{2+} with Pb^{2+} increased the binding affinity of Sp1 for the *APP* promoter. The results revealed that the enhanced interaction force facilitated APP expression and that APP overexpression could confer a high-risk for disease incidence. An increased interaction force between Sp1–f3 and the *APP* promoter in Pb^{2+} solutions was consistent with a lower binding free energy, as determined by computer-assisted analysis. The impact of Pb^{2+} on cell morphology and related mechanical properties were also detected by AFM. The overexpression of APP caused by the enhanced interaction force triggered actin reorganization and further resulted in an increased Young's modulus and viscosity. The correlation with single-force measurements revealed that altered cellular activities could result from alternation of Sp1–*APP* promoter interaction. Our AFM findings offer a new approach in understanding Pb^{2+} associated neurodegeneration.

1. Introduction

Zinc finger transcription factors are essential for regulating the expression of a wide range of genes required for individual development. Specificity protein 1 (Sp1) is a common zinc finger protein that binds with GC-rich regions in promoters and thereby mediates transcription [1]. Its binding with specific DNA sequences facilitates the function of RNA polymerase II and promotes downstream expression. The promoter of the human amyloid precursor protein (*APP*) gene has GC-rich regions, but lacks canonical TATA boxes; thus, *APP* promoter resembles those of housekeeping genes [2]. The essentiality of Sp1 as a mediator of *APP* gene expression has been previously shown. APP overexpression plays a key role in amyloid production during neurodegeneration [3]. The binding sites of Sp1 in *APP* promoter are illustrated in Fig. 1A [4,5]. Transcription is positively regulated by Sp1 [2,6,7]. Some evidence indicates that, during brain development, lead (Pb^{2+}) binds to the Zn^{2+} site of zinc finger proteins. However, experimental data explaining the mechanism of Pb^{2+} involved gene transcription are scarce.

Pb has been considered as an environmental factor that can cause neurodegenerative diseases [8,9]. It is found all throughout the environment, such as industry waste air and contaminated water. High Pb levels in the blood of children remains a serious public health concern [10]. High Pb levels in tap water is a major cause of Pb exposure. Therefore, lots of researches focus on development of new process to remove heavy metal ions from water efficiently and environmentally friendly. A promising approach has been developed to purify

*** Corresponding author.
** Corresponding author.
* Corresponding author.
E-mail addresses: kklyung@hkbu.edu.hk (K.K.L. Yung), peggylo@cityu.edu.hk (P.K. Lo), kinglai@cityu.edu.hk (K.W.C. Lai).

https://doi.org/10.1016/j.abb.2020.108265
Received 20 August 2019; Received in revised form 10 January 2020; Accepted 12 January 2020
Available online 13 January 2020
0003-9861/

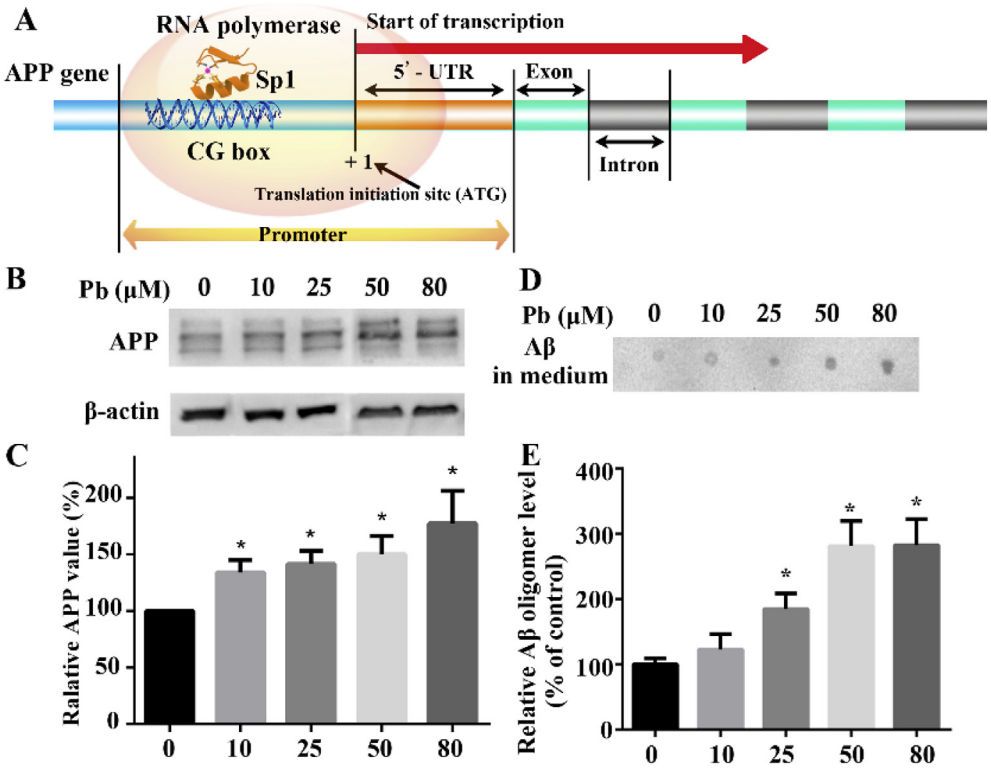

Fig. 1. (A) Mechanism of Sp1-mediated *APP* gene transcription. *APP* mRNA expression by RNA polymerase was positively regulated by binding of the transcription factor Sp1 to the CG box in the *APP* promoter. (B–C) APP accumulation in SH-SY5Y cells after exposure to different Pb^{2+} concentrations for 2 days. APP-expression levels were normalized to β-actin levels. (D–E) Blot dot analysis of the $A\beta_{1\text{-}40}$ secreted in the culture medium (using an anti-$A\beta_{1\text{-}40}$ antibody) and the corresponding quantification of triplicate samples ± SEM. *P < 0.05.

contaminated water via membrane filtration [11]. Amyloid–carbon hybrid membrane has demonstrated a good performance in absorbing heavy metal pollutants like Pb^{2+}. Experiments on animals suggested a statistically significant association between Pb^{2+} exposure and late Alzheimer's disease (AD) onset [12]. AD is believed to be closely related with increased APP production, which can accelerate amyloidogenic peptide deposition in the brain [13]. Rats exposed to Pb^{2+} during development showed elevated APP mRNA expression and Aβ aggregation in late life [14,15]. Furthermore, developmental exposure to Pb^{2+} altered the amount of Aβ in the frontal association cortex [16]. With metal-binding feature, Pb^{2+} also shows the ability to trigger Aβ aggregation. These findings suggest that Pb^{2+} potentially contributes to amyloidogenesis and synapse failure. However, an evaluation of the relevance between AD and Pb^{2+} exposure poses multiple challenges. Zinc level in brain is associated with development and neurodegenerative diseases [17]. Pb^{2+} substitution for Zn^{2+} has occurred in many zinc finger proteins, including Sp1 [18,19]. Pb^{2+} perturbed Sp1 in the cerebellum [20], which plays a critical role in the development of the central nervous system. In addition, studies utilizing nuclear magnetic resonance (NMR) have provided powerful evidence that Pb^{2+} binds to the Zn^{2+} binding site of Sp1 [18]. Thus, we proposed that substitution of Zn^{2+} with Pb^{2+} in Sp1 upregulates *APP* transcription and causes Aβ production in the brain. Many techniques, such as electrophoretic mobility-shift assay (EMSA) [21] and DNA footprinting [22], can be used to characterize protein–DNA associations. However, the band intensity obtained from these methods cannot explain the unbinding force occurring in stochastic dissociation processes. Thus, we applied atomic force microscopy (AFM) to investigate the unbinding force in detail.

In vitro studies have provided insights into the functional activities of APP. These activities are one of the important factors in the migration of neuronal precursors during brain development [23]. Studies on cultured neurons showed that APP is involved in neurite outgrowth [24,25] and cell migration [26]. A certain amount of APP at the cell surface might affect cell movement by regulating actin polymerization [27]. Previous findings showed that APP mediated cell-to-cell and cell-to-matrix adhesions via large extracellular domains [28]. Cellular mechanical properties can be altered during these physiological activities. However, correlations between APP levels and cellular mechanical properties remain elusive despite extensive efforts in elucidating the biological functions of APP in plasma membranes.

In this study, we focused on the interaction between Sp1–f3 and the *APP* promoter in the presence of solutions containing different ion concentrations, and the impact of the altered interactions on the cellular activities. Considering that expression of the *APP* gene can be mediated via Sp1, we were able to directly study interference of the Sp1–DNA interaction by Pb^{2+} or Zn^{2+} *in vitro*. We performed experiments to test the unbinding force of Sp1–f3 on a DNA fragment containing a CG box element in the *APP* promoter region in the presence of various ions, using AFM spectroscopy. The unbinding force measured in the presence of Pb^{2+} significantly increased relative to that in the presence of Zn^{2+}. This phenomenon can be explained by Pb^{2+} occupying the position of Zn^{2+} in Sp1, which strengthened the binding capability. Computer-assisted studies on the *APP* promoter revealed a reduced binding energy, which supported our experimental data. These results suggest that Pb^{2+} and Zn^{2+} can compete at the zinc finger domain, which affects Sp1–DNA binding and results abnormal gene regulation. Pb^{2+}-induced perturbation in Sp1 binding with a target DNA sequence can cause various adverse effects, including altered APP expression and mechanical properties.

2. Results and discussion

2.1. Pb^{2+} associated with translation of the APP gene

Aβ accumulation initiates a cascade of events that causes neuropathological changes. Increased APP production may positively affect amyloid plaque deposition. To test the relationship between Pb^{2+} exposure and relative protein expression, we exposed human SH-SY5Y neuroblast cells to $PbCl_2$ and monitored APP expression. Western blot analysis showed that a proportion of APP was associated with the concentration of Pb^{2+}. As shown in Fig. 1B and C, the APP protein level in SH-SY5Y cells increased in a concentration-dependent manner after 2

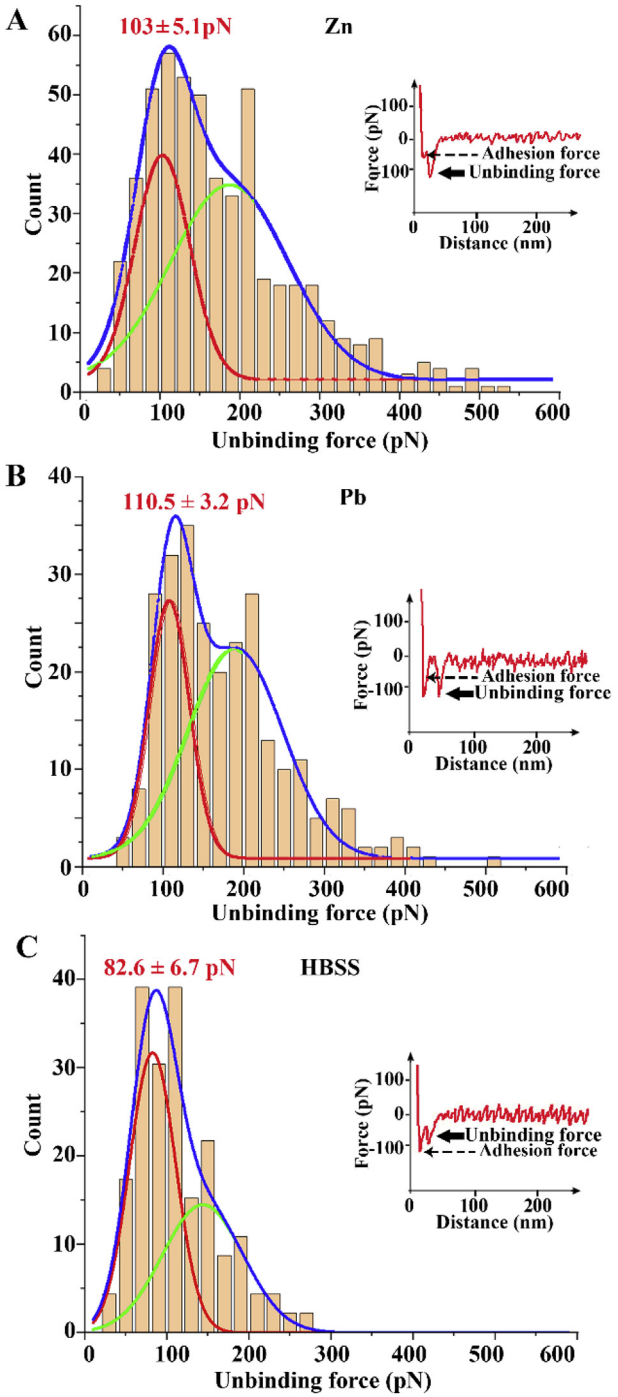

Fig. 2. Histograms showing unbinding-force distributions in the presence of (A) Zn^{2+} ion, (B) Pb^{2+} ion, and (C) HBSS. Each curve represents a Gaussian-fitted result. The insets show representative force curves obtained from *APP* promoter-functionalized tips and Sp1–f3 in buffer solution containing Zn^{2+} or Pb^{2+}. Arrows indicate unbinding events.

days of incubation. When 10, 25, 50, or 80 μM Pb^{2+} was added to the culture medium, the average APP production increased by 17%, 30%, 34%, or 71%. As shown in Fig. 1D–E, a similar trend was observed for $A\beta_{1\text{-}40}$. Cell viabilities were determined by performing 3-(4,5-dimethylthiazol-2-yl)-2,5-diphenyltetrazolium bromide (MTT) assays (Fig. S1). Unlike the control cells, the cellular physiological activity was not affected when the Pb^{2+} concentration reached 80 μM. These observations support our findings on the role of Pb^{2+} in accelerating APP expression and Aβ secretion.

A series of evidences suggest that neurodegenerative disorders are caused by heavy metals, such as Cu^{2+}, Fe^{2+} and Pb^{2+} [29,30]. It has been demonstrated that Pb^{2+} exposure in early life causes neuropathological changes [31]. Rat pheochromocytoma cells exposed to Pb^{2+} showed concentration-dependent increases in APP mRNA and Aβ peptide expression [32]. Much research has focused on the molecular mechanism of Pb^{2+}-induced developmental neurotoxicity. These mechanisms may involve alterations in gene transcription, which are essential for physiological activities. Previous evidence showed that substituting Zn^{2+} with Pb^{2+} in zinc finger proteins can cause and exacerbate neurodegeneration [18,19]. In addition, recent findings revealed that Pb^{2+} can interfere with cell growth and differentiation by interacting with the transcription factor Sp1 [20]. Pb^{2+} interference can modulate the binding capability of Sp1 to its specific target DNA sequence [33]. Pb^{2+} exposure during development can also transiently increase interactions between Sp1 and target DNA [20] when combined with a brief increase in APP mRNA expression [30,33]. We propose that Pb^{2+} can induce a transient increase in the binding of Sp1 to DNA, thereby enabling Sp1 to increase the transcription of specific genes, such as *APP*.

2.2. Estimation of the unbinding force between Sp1–f3 and the APP promoter

Pb^{2+} exposure promotes APP expression in neuronal cells. Furthermore, enhanced binding of the transcription factor Sp1 is associated with upregulated *APP* expression [30]. In molecular-dissociation processes, an applied force is required to overcome an energy barrier [34]. A higher-level energy barrier indicates a relatively strong binding activity between two molecules. The unbinding force, which can be determined by AFM, is proportional to the energy barrier [35]. AFM-based measurements can be used to effectively characterize multiple parameters in biological systems [36]. The unbinding force was identified as a disease biomarker. For instance, the unbinding force has been used to quantify the interaction between fibrinogen and erythrocytes [37], the interaction of DNA with a specific binding protein [38], and the strength of peptide aggregation [39].

We propose that Pb^{2+} can enhance the DNA-binding activity of Sp1, which might promote APP expression as shown aforementioned. Therefore, we conducted independent AFM experiments to measure the interaction between the *APP* promoter and Sp1–f3 in buffered solutions containing Zn^{2+} or Pb^{2+}. The experimental procedure used to measure the unbinding force between the third finger of Sp1 and CG box in the *APP* promoter by AFM is depicted in Fig. S2. At the beginning of the retracing process (i.e., stage 1), the AFM cantilever deflects upward when the APP-functionalized AFM tip binds Sp1–f3. Then, the AFM tip is withdrawn, and the adhesion force is usually detected in stage 2. This downward peak in the contact region is an indicator of the adhesive force between the tip and the sample surface. The AFM tip remains in contact with the sample surface at this stage. In stage 3, molecular interactions occur and cause a downward bending of the cantilever in the non-contact region. Then, the binding between Sp1–f3 and the target DNA is ruptured and the cantilever is reverted. In stage 4, the cantilever returns to a relaxed state without deflection. To facilitate the formation of a stable protein structure with various ions, we pre-incubated the Sp1–f3-modified substrate with Zn^{2+}, Pb^{2+}, or Hank's balanced salt solution (HBSS). AFM spectroscopy was employed to detect the interaction force between Sp1–f3 and double-stranded DNA from the *APP* promoter. Fig. 2 shows a histogram of the unbinding force required to break the binding between the *APP* promoter and Sp1–f3 in different solutions, namely, a normal group (Zn^{2+}) and a treatment group (Pb^{2+}). The data were fitted to a Gaussian distribution to obtain the most probable force for the Sp1–f3–DNA combination. The histograms showed multiple peaks, indicating that multiple unbinding events were detected. A possible explanation for the observation of multiple peaks is that the AFM probe bound multiple pairs of molecules simultaneously.

The value of the first Gaussian-fitted peak in the histogram represents the average unbinding force. Representative force–distance curves under different conditions are shown in the insets. When no specific recognition occurs, an adhesion force can be observed in the force–-distance curve; otherwise, the force is an unbinding force. The first peak in each curve represents an adhesion force. At a certain distance from the contact point, the unbinding force is depicted by the second peak (which is separated from the first peak). The unbinding forces for the Sp1–f3–DNA complexes in the presence of HBSS, Zn^{2+}, and Pb^{2+} were 82.6 ± 6.7, 103.1 ± 5.1, and 110.5 ± 3.2 pN, respectively. The strongest Sp1–f3–*APP* promoter interactions were measured with the treatment group (Pb^{2+}), followed by the normal group (Zn^{2+}) and the control group (HBSS). The Sp1–f3–*APP* promoter complex in Pb^{2+} solution has a higher unbinding force than in Zn^{2+} solution. Thus, we conclude that Sp1–f3 has a higher binding capacity in the presence of Pb^{2+} than in the presence of Zn^{2+}. The results indicate that the force required for Sp1–f3 dissociation from the *APP* promoter depends on the ion type. The transcription process can be facilitated by the surrounding ions, where an increased binding capability is associated with higher transcription. EMSA was also conducted to verify the protein–nucleic acid interactions, as previously reported [21]. Sp1–f3 can bind to the DNA fragment from the *APP* promoter (Fig. S3).

Changes in Sp1–f3–*APP* promoter interactions can provide insights into pathogenesis and pathological development. AFM was utilized to evaluate and characterize the changes in the interaction force between Sp1–f3 and the *APP* promoter in different solutions. Molecules were end-immobilized on the AFM tip and the substrate. This scheme enabled us to measure DNA–protein interactions at the single-molecule level. The unbinding force in buffered solution containing Pb^{2+} was significantly higher than that in buffered solution containing Zn^{2+}. Pb^{2+} exposure may promote Sp1 binding to the *APP* promoter and contribute to higher APP expression, which is associated with Aβ production. The specific interaction was evaluated by EMSA, as previously described. Moreover, the exact unbinding force was studied and found to increase dramatically after exposure to Pb^{2+}. The Sp1–f3–*APP* promoter complex showed a stronger binding affinity in the presence of Pb^{2+} versus Zn^{2+} or HBSS. These results accord well with our previous Western blot data, where a higher binding affinity corresponded to higher protein expression. The above evidence indicates that alterations in the interaction force can potentially explain Pb^{2+}-induced disease.

2.3. Sp1 specifically bound to the APP promoter

The transcription factor Sp1 binds with the CG box in various promoters and controls the transcription process. In this study, AliBaba software, version 2.1 was used to predict the Sp1-binding sites in the APP promoter (http://www.gene-regulation.com/pub/programs/alibaba2/index.html) [40]. Analysis of the binding segments suggested that Sp1 potentially binds the *APP* promoter. It was reported that Pb^{2+} induces amyloidogenic pathways and Aβ aggregation [41]. Amyloid protein present several binding sites with heavy metal ions [11,42]. We first verify the interaction between APP and heavy metal (Zn^{2+} and Pb^{2+}) as aberrant metal homeostasis in patients with AD. Binding isotherm result is shown in Fig. S4. Not only binding with APP, NMR spectroscopy has demonstrated that Pb^{2+} interferes with binding of the zinc finger domain, which is critical for Sp1–DNA complex formation. To fully understand the mechanism whereby Pb^{2+} may alter the binding activity of Sp1 and (in turn) modulate gene expression, we examined the effects of Pb^{2+} on the binding capacity of Sp1–f3 with its DNA consensus sequence, which was derived using the Amber 17 software package. The third-finger domains (Sp1–f3) strongly contributed to specific interactions in a previous study [43]. Hence, we used the last zinc finger domain in the simulation. The structure was solved using standard homonuclear two-dimensional NMR techniques [44]. The structures of the complex in the presence of Zn^{2+} or Pb^{2+} are shown in Fig. 3A and 3B. The root-mean-square deviations (RMSD) of

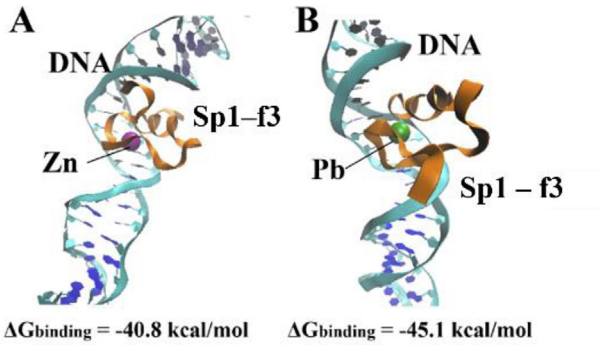

Fig. 3. Structure of the Sp1–f3–*APP* promoter complex after 30 ns of molecular dynamics simulation. The purple sphere represents the Zn^{2+} ion (A), and the green sphere represents the Pb^{2+} ion (B). (For interpretation of the references to colour in this figure legend, the reader is referred to the Web version of this article.)

the coordinates in the equilibration period are demonstrated in Fig. S5. For the Sp1–f3–*APP* promoter complex in the presence of Zn^{2+}, the RMSDs of all molecules increased within the first 2 ns. The RMSD values varied from 0.25 nm to 0.75 nm. This increase indicates that large changes occurred in the structure of the complex. Between 2 ns and 30 ns, the RMSD values fluctuated at 0.78 ± 0.08 nm, which suggest a remarkably stable behavior. For the complex in the presence of Pb^{2+}, the RMSD value increased from 0.4 nm to 0.7 nm at the beginning of the process. Furthermore, the plot was stable during the first 1 ns and presented small deviations at subsequent simulation times. The complex systems equilibrated rapidly in both cases. Then, the binding free energy ($\Delta G_{binding}$) was identified from the same simulation. $\Delta G_{binding}$ for the DNA–protein complex in the presence of Zn^{2+} or Pb^{2+} was −40.8 kcal/mol or −45.1 kcal/mol, respectively. $\Delta G_{binding}$ was previously proposed to reflect the stability of protein–nucleic acid complexes [45]. The energy difference for complex binding with Zn^{2+} or Pb^{2+} was −4.3 kcal/mol. The reduced energy of the protein–DNA complex in the presence of Pb^{2+} drove their binding and facilitated molecular interactions. The Sp1–f3–*APP* promoter complex was more stable in Pb^{2+} solution than in Zn^{2+} solution. The stabilizing effect of Pb^{2+} on the zinc finger–DNA complex can be attributed to the lower binding free energy. The finding is consistent with the results for the corresponding unbinding force, where the force required to break the interaction between Sp1–f3 and the *APP* promoter in the presence of Zn^{2+} was smaller than that in the presence of Pb^{2+}. Altering this binding affinity increased the production of APP and its cleavage product, Aβ.

2.4. Determining the cellular mechanical properties and morphology

The physiological activities of cells can influence the cellular mechanical properties. The presence of APP in a cell membrane is closely related to cell mechanics during the migration process [27]. In this study, we aimed to correlate mechanical changes in SH-SY5Y cells with Pb^{2+} exposure and APP expression. AFM-based nano-indentation was applied to measure the cellular Young's modulus and viscosity values (Fig. 4). Young's modulus increased after exposure to Pb^{2+} when compared to that of the control group. Among the three treatments, the cells incubated in 80 μM Pb^{2+} were the stiffest (Young's modulus, 2.70 ± 0.26 kPa). These findings agree well with previous reports on the stiffening of erythrocytes in workers exposed to lead [46]. Cells are considered viscoelastic materials in physiological environments. They show elastic responses and display time-dependent responses to mechanical stimulation. These time-dependent mechanical responses can be utilized to examine changes in cell viscosity [47]. Hence, cells were modeled using a standard linear, solid model that combined a spring damper in parallel with another spring, as described in previous

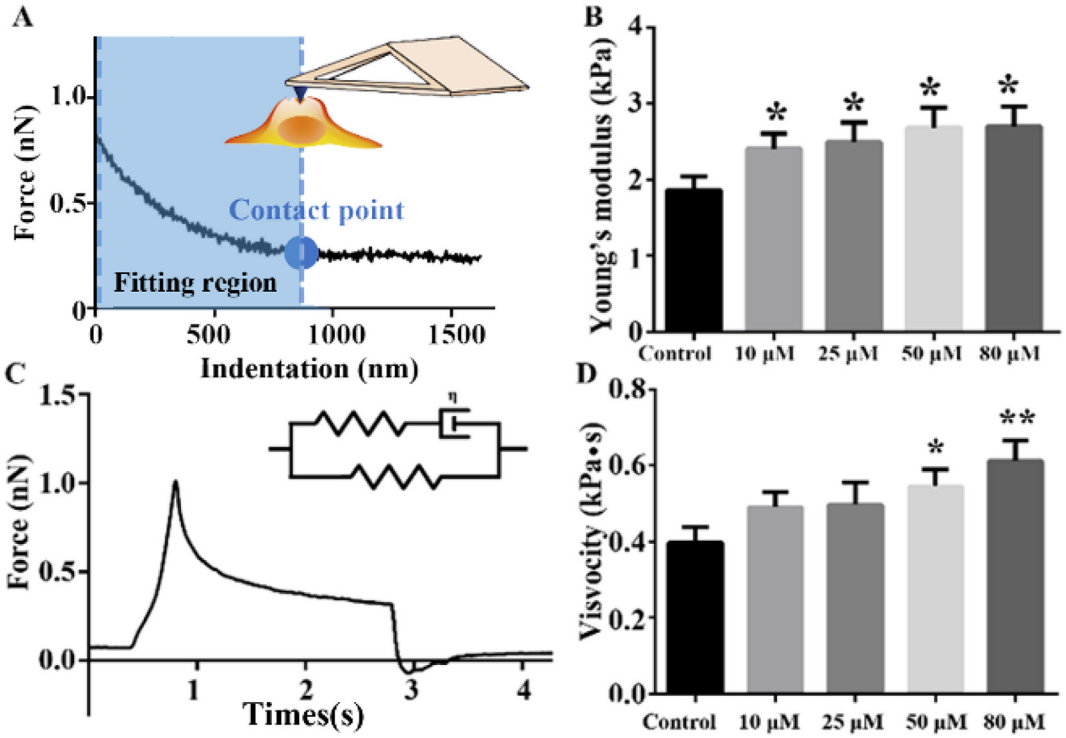

Fig. 4. (A) Representative force–distance curve obtained using SH-SY5Y cells. The inset image is a schematic representation of an AFM-based nano-indentation measurement. (B) Young's modulus of cells incubated with different concentrations of Pb^{2+}. (C) Representative stress–relaxation profile of control cells. The inset image is a viscoelastic model. (D) The viscosity of cells incubated with different concentrations of Pb^{2+}. The data shown are expressed as the mean ± SEM. *P < 0.05; n > 30.

research [48]. Cells incubated in the presence of 80 μM Pb^{2+} showed the highest viscosity at 10.2 ± 2.7 Pa s. Fig. 4D shows the impact of different Pb^{2+} concentrations of cell viscosity compared with the control group. Our data revealed a strong relationship between APP overexpression and the mechanical performance of SH-SY5Y cells.

Cellular viscoelasticity is caused by cytoskeletal relaxation. The Pb^{2+}-induced increase of Young's modulus was likely caused by APP overexpression, which tended to change the architectural features of the actin cortex [49]. To observe the cortical actin in detail, we employed AFM measurements to process the images of the cell membrane surface, which provided high-resolution visualization. We then analyzed cell morphology in the presence or absence of Pb^{2+} using AFM. The AFM images are shown in Fig. 5A–F. We selected small square areas (5 μm × 5 μm) to obtain a clear image. The filaments on the cell surface represent the actin cortical cytoskeleton (Fig. 5G–L). The control cells were evenly distributed in a relatively homogeneous cell population. The actin cytoskeleton was organized with thick fibers connected with each other at actin branch junctions. However, changes in the cell surface began to appear at a Pb^{2+} dose of 10 μM. Cells exposed to 10 and 25 μM Pb^{2+} acquired an increased number of membrane folds, which were supported by the actin cytoskeleton [50,51]. These folds were positioned parallel to one other. In addition, the surface changes in SH-SY5Y cells were qualitatively proportional to the concentration of Pb^{2+} to which the cells were exposed. A coarse mesh (arrowheads in Fig. 5I) was discernible when the Pb^{2+} concentration reached 50 μM. The mesh size ranged from 0.5 μm to 1 μm. The number of these mesh-like structures was related to the Pb^{2+} concentration. The actin meshwork became much smaller and dramatically denser at a Pb^{2+} concentration of 80 μM (Fig. 5J). It has been demonstrated that actin is the most significant component responsible for morphological images observed by AFM [52]. The pattern of actin filaments in the cortex was likely related to the degree of APP expression. Thus, the biophysical effect of the Pb^{2+} ion on cellular mechanical properties may have resulted from the reorganization of actin filaments.

Pb^{2+}-induced changes in the binding activity of Sp1, which can alter protein expression and subsequent activities, are illustrated in Fig. 6. Increased formation of amyloidogenic Aβ products can be observed at elevated Pb^{2+} concentrations, which induce alterations of cellular activities. Fully understanding the biological functions of APP in normal nervous systems and in pathophysiological situations, such as AD, is imperative. Cellular mechanics have been characterized in studies of cellular physiology [47]. The cross-linking activity of actin filaments underlying the cell membrane has a positive effect on cortical mechanics [53]. APP participated in cell migration by modulating FE65. Formation of the APP–FE65 complex assists in the regulation of cell movement by changing actin-based motility [27]. Mechanical changes caused by actin dynamics can be detected by AFM-based nano-indentation experiments. Marked increases of Young's modulus and viscosity were identified after Pb^{2+} exposure, which can be attributed to actin reorganization. Changes in mechanical properties were pronounced during disease progression [54]. The relationship between cell mechanical characteristics and cell ultrastructural architecture was revealed in a previous study [55]. Given that Pb^{2+} exposure can alter cell morphology [56,57], AFM was selected to measure the cell morphology after exposure to Pb^{2+}. In our AFM images, distinguishable meshwork features can be observed on the cell membrane. Dynamic changes in the organization of actin networks and the Pb^{2+} concentration were positively correlated. Our observations were consistent with those of another study, in which the meshwork density increased after jasplakinolide treatment [58].

3. Conclusions

Several complementary techniques, such as AFM spectroscopy, Western blot analysis, and computer-assisted simulations, were utilized to reveal the relationship between Pb^{2+} exposure and the mechanical properties of transcription. AFM spectroscopy was applied to evaluate changes in the interaction between the transcription factor Sp1 and the

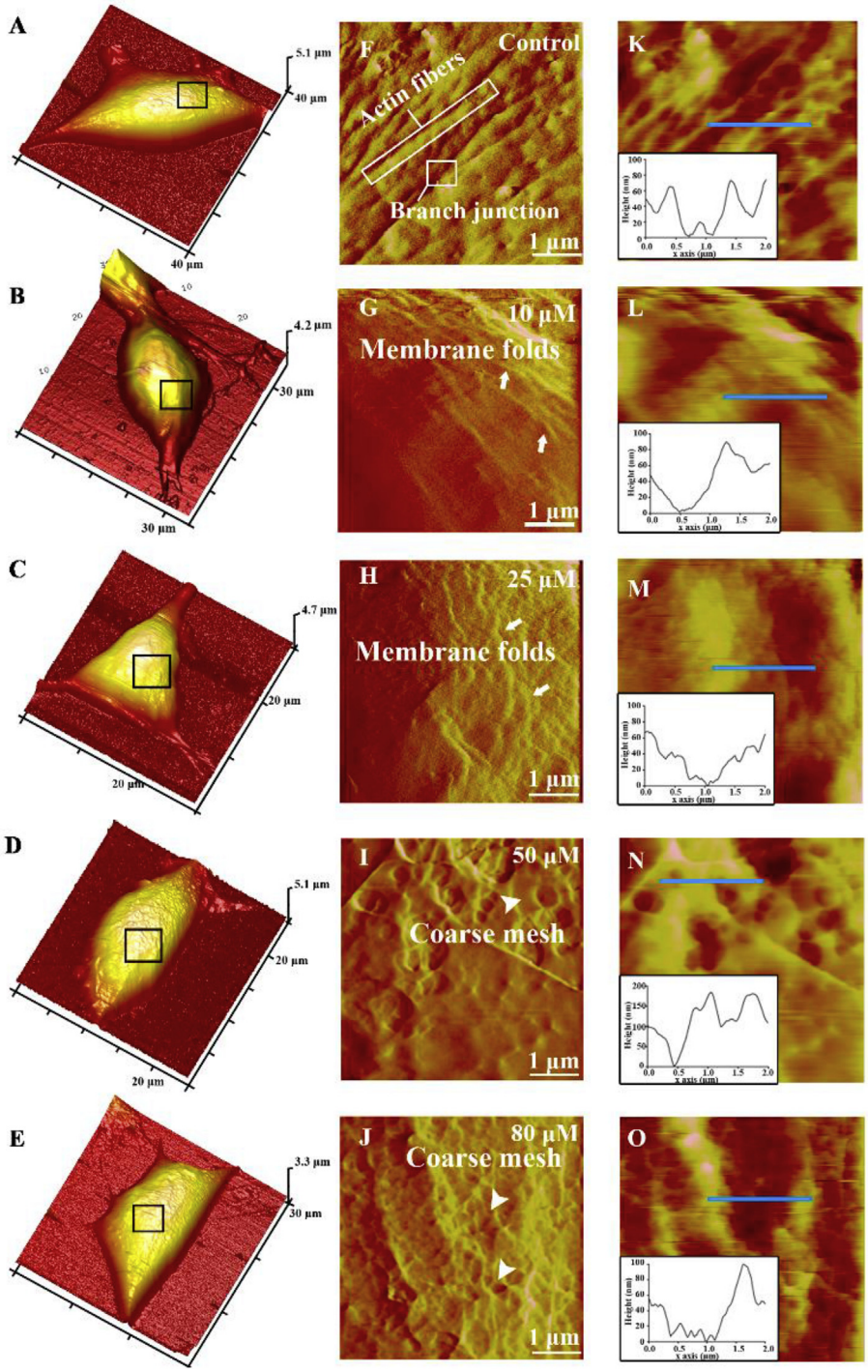

Fig. 5. AFM images of SH-SY5Y cells after exposure to different Pb^{2+} concentrations for 2 days. (A–E) Three-dimensional height images of normal SH-SY5Y cell and Pb^{2+}-exposed SH-SY5Y cells. (F–J) Peakforce error images observed after zooming in on the small square areas shown in panels A–E. (F) Regular actin organization was found in control cells. (H–I) Parallel membrane folds were observed on the cell membranes (arrows) in the presence of 10 μM and 25 μM Pb^{2+}. (I–J) Coarse mesh (arrowheads) were discerned on the cell membranes after treatment with high concentrations of Pb^{2+}. (K–O) AFM height image observed after zooming in on the small square areas shown in panels A–E. The insets show the AFM cross-section analysis.

APP promoter. Occupation of the Zn^{2+}-binding site in Sp1 with Pb^{2+} might promote Sp1 binding to the *APP* promoter, which accelerates *APP* gene expression during development. Environmental interferences alter APP expression and processing during human development, which potentially has a positive influence on the level of amyloidogenesis. Our current work provides the evidence of the impact of Pb^{2+} on the related biophysical properties. Exploring the molecular mechanisms that underlie the interaction between Sp1 and the *APP* promoter is important for future drug discovery and therapy.

4. Experimental methods

4.1. Materials

Boric acid, urea, ethylenediaminetetraacetic acid disodium salt dihydrate (EDTA), formamide, acrylamide, bis-acrylamide, ammonium persulfate, tris(hydroxymethyl)aminomethane (Tris), and *N*,*N*,*N*′,*N*′-tetramethylethylenediamine (J&K Scientific Ltd., China) were used to prepare the DNA sequences. For automated DNA synthesis, 1000 Å nucleoside-derivatized LCAA-CPG and 3′-amino-modified C7 CPG solid supports were used (Beijing DNAchem Biotechnology Co., Ltd, China), with loading densities of 25–40 μmol/g. Sephadex G-25 was applied for affinity chromatography (superfine DNA grade, Amersham Biosciences,

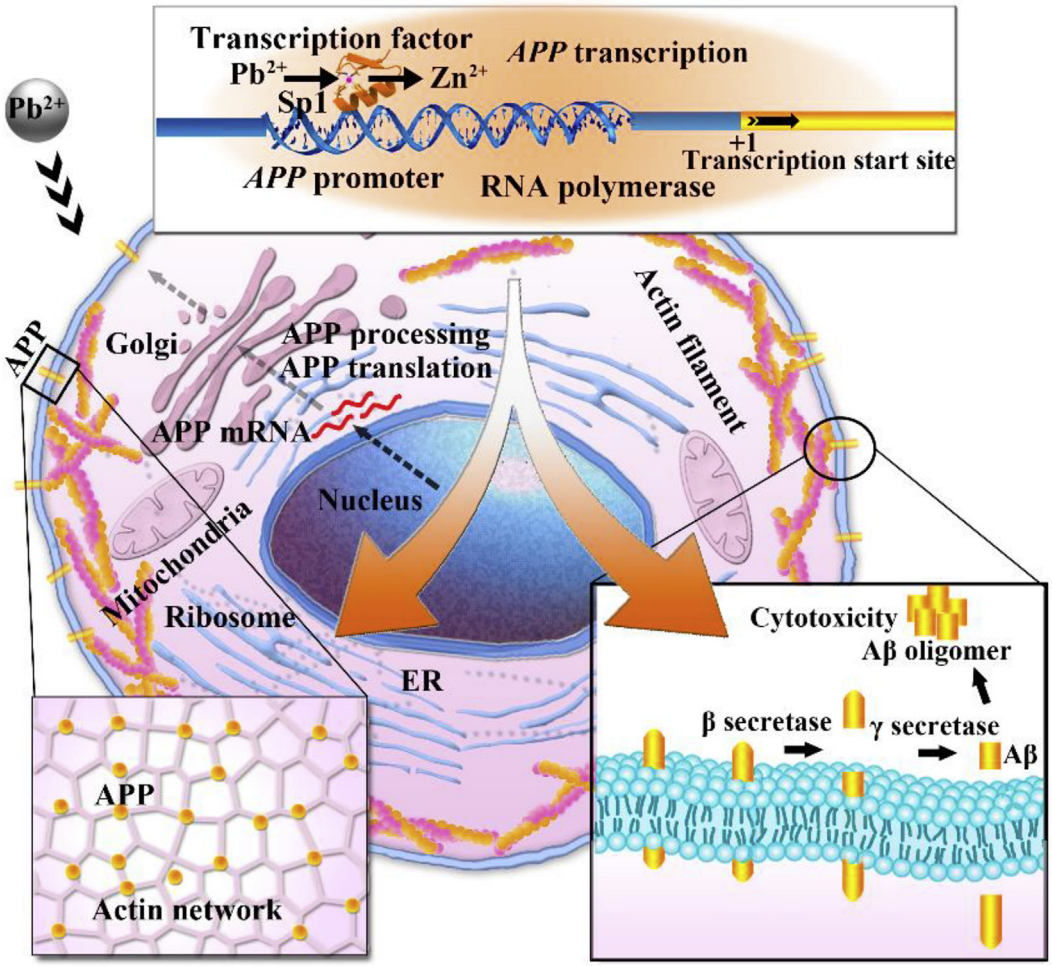

Fig. 6. Schematic representation of APP expression in cells exposed to Pb^{2+}. Pb^{2+} can substitute for Zn^{2+} in Sp1, a transcription factor that helps in the recognition of gene promoters. The top box depicts Sp1-dependent transcriptional activation by RNA polymerase II. Pb^{2+} stimulates the activity of Sp1, which facilities APP expression. APP overexpression regulates actin dynamics and promotes actin polymerization. Then, altered actin organization leads a meshwork structure on the cell membrane. The formation of Aβ by cleavage of APP with β-secretase is also depicted. Subsequently, the Aβ fragment is cleaved by γ-secretase, which generates Aβ isoforms ranging from 36 to 43 residues in length.

USA). The 1 × TBE buffer used in our experiments was composed of 90 mM Tris, 90 mM boric acid, and 1.1 mM EDTA, and had a pH of ~8. Molecular biology-grade agarose was obtained from Vivantis Technologies (Malaysia). ShinyGreen™ Safe DNA Dye, 20,000 × in water (Thermo Fisher Scientific, USA) was used to view DNA.

4.2. Zinc finger and APP promoter preparation

A synthetic peptide, corresponding to the third zinc finger motif of Sp1 (KFACPECPKRFMRSDHLSKHIKTHQNKK), was obtained from Top peptide Co. Ltd (China), at a purity of 97.89%. The amino acid sequence of the peptide was based on information deposited in the NCBI database.

A fragment containing 48 base pairs of the *APP* gene promoter (5′-GCAGCAGTCCTTTATACGACACCCCCGGGAGGCCTGCGGGGTCG GAT-3′) displayed high promoter activity. Standard solid-phase oligonucleotide synthesis was performed on a BioAutomation MerMade MM6 DNA synthesizer, and the synthesized DNA samples were deprotected in concentrated ammonium hydroxide solutions. Crude DNA strands were purified on 15% polyacrylamide/8 M urea polyacrylamide gels in 1 × TBE buffer on a 20 × 20 cm Maxi Vertical electrophoresis apparatus (MV-20DSYS). DNA concentrations were measured in a NanoDrop ND-1000 spectrophotometer. The double-stranded DNA promoter was prepared by annealing complementary strands in 1 × PBS buffer in a Hercuvan Lab System Pro Gradient Touch Thermal Cycler, using an annealing temperature that decreased from 95 °C to 4 °C over 5 h. Correct synthesis of the amino-modified DNA was confirmed by matrix-assisted laser desorption-ionization time-of flight mass spectrometry (MALDI-TOF MS). The molecular weight of the amino-modified DNA was calculated to be 14691.58 g/mol, which agreed well with the experimentally determined value of 14703.7164 g/mol (Fig. S6).

4.3. EMSA experiments

Agarose gel electrophoresis was performed on Bio-Rad Mini-Sub Cell GT Cell Apparatus with a 7 × 7 cm gel tray (Bio-Rad, USA). Agarose gels were scanned using a Bio-Rad ChemiDoc™ Touch Imaging System. MALDI-TOF MS was performed on a Bruker Autoflex Mass Spectrometer (Bruker Co., USA).

4.4. Binding isotherms

Recombinant APP was purchased from R&D System. Metal cation affinities to APP were determined by UV–Vis spectroscopy. APP solution (1.3 μM) were titrated by various concentration of heavy metal. The binding isotherms were fitted using Langmuir binding model.

4.5. AFM tip functionalization

DNP-10 probes (Bruker Co., USA) were used in the AFM tip-functionalization experiments. The probes were made of silicon nitride cantilevers with silicon nitride tips. The spring constants were measured by the thermal-fluctuation method before each experiment and ranged from 0.04 N/m to 0.21 N/m. First, the tips were placed in a plasma reactor (Oxford PlasmaLab 80 Plus RIE System) with a highly purified oxygen gas atmosphere for 2 min to obtain hydroxyl surfaces. Tips were silanized in a vacuum chamber containing (3-Aminopropyl) triethoxysilane (APTES) and trimethylamine (Sigma, USA) for 3 h. The tips were then placed in a crosslinker solution (2.5% glutaraldehyde [vol/vol]) and incubated for 40 min. After reaction, the tips were gently washed three times with PBS. Finally, the DNA molecules were immobilized on the surface by placing the tips in promoter solution and immediately mounted on AFM for the spectroscopy experiments.

4.6. Preparation of Sp1-f3 substrate

Silicon wafers were used as the substrate. We first cleaned the substrates with ethanol and acetone. After rinsing them with deionized water, the substrates were dried under compressed air. Then, modification procedures were applied as for the tip functionalization. After glutaraldehyde was covalently attached to the silicon substrates, they were immersed in Sp1–f3 solution to link the Sp1–f3 molecules. Prior to performing the experiments, the Sp1–f3-modified substrates were pre-incubated with PBS supplemented with Zn^{2+} or Pb^{2+}, at a concentration equaling that of Sp1–f3.

4.7. AFM-based spectroscopy

AFM measurements were conducted on a Biocatalyst system (Bruker Co., USA) in a liquid environment at room temperature. The retraction speed of the AFM probe was set to 1 μm/s. Experiments were performed 3 times under each condition. In each experiment, approximately 1000 force–distance curves were collected. According to the accuracy of instrument, force values up to 20 pN were considered as noise or artifacts. Statistical analysis was performed using Student's *t*-test.

4.8. Cell culture

Human neuroblastoma SH-SY5Y cells were cultured in 2.5-cm^2 flasks in complete medium, which was DMEM/F12 supplemented with 10% fetal bovine serum and a 1% antibiotic mixture (Penicillin-Streptomycin-Neomycin; Thermo Fisher Scientific). A stock solution of 10 mM lead chloride was prepared in sterile distilled water for treatments. Working solutions were diluted in DMEM/F12 media for the different exposures. For further research on APP expression, SH-SY5Y cells were grown in 6-well plates and incubated in basic culture medium containing 10 μM, 25 μM, 50 μM, or 80 μM Pb^{2+}. The sodium concentration in the culture medium was much higher than the Pb^{2+} concentration. We thus ignored the influence of osmolality caused by Pb^{2+}.

4.9. Western blot analysis

Cells were lysed with protein extraction reagent (Novagen Co. Ltd, USA) supplemented with protease inhibitor cocktail (Calbiochem, USA). After separating cellular fragments from lysates, each supernatant was denatured and separated by 10% sodium dodecyl sulfate-polyacrylamide gel electrophoresis. The proteins were then transferred to a polyvinyl difluoride membrane and blocked for 1 h with 5% skim milk. Subsequently, the membrane was immunoblotted with an anti-APP antibody (ab32136, Abcam, USA). After incubation for 2 h, the membranes were washed three times with Tris Buffered Saline with Tween 20 (TBST) and incubated with specific secondary antibodies, and the bands were visualized with ChemiDoc Touch imaging system (Bio-Rad, USA). APP protein levels normalized to β-actin expression (A2228, Sigma, USA), which was detected as a reference.

4.10. Dot blot analysis

Dot blots were performed with 3 μg of protein per sample, using an anti-amyloid beta antibody (ab76317, Abcam, USA) as described previously [59]. The dot blots were used to quantify secretion of the $A\beta_{1\text{-}40}$ peptide into the culture medium. After the spots were air-dried, the membranes were processed as described above for the western blots.

4.11. Measurement of cellular mechanical properties

To explore the cellular mechanical properties, contact mode in fluid was applied based on previously described procedures [60]. The Sneddon model was chosen as the fitting model to calculate the Young's modulus of cells. A trigger force of 1.5 nN was applied to deform the cells. In our case, this force caused a 0.5–1 μm indentation, which corresponds to less than 15% of the cell height. The half angle (α) of the AFM tips (DNP-D probe) was set to 18°, and the Poisson ratio (ν) was assumed to be 0.5. The AFM probe was aligned to the center of each cell, and approximately 9 force–distance curves were collected per cell, using the following equation:

$$F = \frac{2}{\pi}\frac{E}{1-\nu^2}\delta^2 \tan\alpha$$

where F represents the loading force, E is Young's modulus, and δ is the indentation depth.

Cellular viscosities were determined by performing stress–relaxation tests. In our experiments, after the tip reached the trigger force, the AFM cantilever was held at a constant displacement for a specific relaxation time (2 s). The corresponding force response over time was monitored with an oscilloscope. The applied force decayed exponentially when the tip was indented into the cell, and the stress–relaxation curves were fit with the following exponential equation:

$$\frac{F(t)-F_{final}}{F_{initial}-F_{final}} = e^{-\frac{Et}{\eta}}$$

where t is the testing time and η represents the cellular viscosity [48,61].

For each condition, at least 30 cells were tested to obtain sufficient results for statistical analysis using Student's *t*-test. The indentation function in Nanoscope v1.5 was applied to fit the force–distance curves. Data analysis was performed by MATLAB, Nanoscope v1.5, and GraphPad Prism.

4.12. Cell morphology measurements

All cells were investigated with a BioScope Catalyst AFM (Bruker Co., USA) in Peakforce Tapping mode in liquid. An OLTESPA probe was applied to obtain cell images. The cells were first incubated with different concentrations of Pb^{2+} for 2 days. Then, the cells were fixed with 4% paraformaldehyde for 30 min and washed with HBSS. In our AFM imaging experiments, the loading force was set to 6 nN and the scan rate was set to 0.3 Hz.

4.13. Cell-viability assays

Cell viabilities were measured using MTT (M2128, Sigma). The cells were treated as indicated. Next, 20 μl of the MTT assay reagent (5 mg/ml) was added to each well. After 4-h incubation with the MTT reagent, medium was removed. Dimethyl sulfoxide was then added to each well to soluble the formazan crystals. The absorbance was read at 490 nm. The cell viabilities were normalized to the control group. The data were analyzed using GraphPad Prism.

4.14. Molecular dynamics simulations

DNA strands were generalized using AMBERTools17. Crystal structure of Sp1-3 (1SP1 [62]) was retrieved from the Protein Data Bank. Molecular dynamics simulations were performed with the Amber 17 software package. The simulation consisted of five stages, namely minimization, heating, equilibration, MD simulation, and analysis. The energy of the whole system was minimized with 5,000 cycles of steepest descent and 5,000 cycles of conjugate gradient (a non-bonded cut-off of 10 Å was applied). Then, the complex was heated to the desired temperature (300 K) gradually within 50 ps at a 2 fs time step. After heating, our system was equilibrated at a constant pressure for 50 ps. Finally, molecular dynamics simulations were performed for 30 ns. After completing the simulation, trajectory analysis was performed, which generated numerous frames. Six hundred snapshots at an interval of 50 ps were extracted from the 30 ns trajectory. The cpptraj module was used to evaluate the RMSD values. The Molecular Mechanics Generalized Born Surface Area (MMGBSA) method was used to calculate binding free energy between DNA and protein.

CRediT authorship contribution statement

Qi Gao: Investigation, Visualization, Writing - original draft, Conceptualization. **Ziwen Dai:** Investigation, Visualization. **Shiqing Zhang:** Investigation, Visualization. **Ken Kin Lam Yung:** Supervision, Methodology. **Pik Kwan Lo:** Supervision, Methodology. **King Wai Chiu Lai:** Conceptualization, Methodology, Supervision, Writing - review & editing.

Declaration of competing interest

The authors report no declarations of interest.

Acknowledgements

This work was supported in part by the Research Grant Council of the Hong Kong Special Administrative Region Government under Grant CityU139313, Grant CityU11205815, Grant CityU11205514, and the CityU Research Grant 7004854, Grant 9667166, Grant 7005119.

Appendix A. Supplementary data

Supplementary data to this article can be found online at https://doi.org/10.1016/j.abb.2020.108265.

References

[1] R.K. Kothinti, A.B. Blodgett, D.H. Petering, N.M. Tabatabai, Cadmium down-regulation of kidney Sp1 binding to mouse SGLT1 and SGLT2 gene promoters: possible reaction of cadmium with the zinc finger domain of Sp1, Toxicol. Appl. Pharmacol. 244 (2010) 254–262, https://doi.org/10.1016/j.taap.2009.12.038.

[2] W.J. Lukiw, E.I. Rogaev, G. Vaula, P.S. George, T.N. Building, Protein-DNA interactions in the promoter region of the amyloid precursor protein (APP) gene in human neocortex, Mol. Brain Res. 22 (1994) 121–131.

[3] D.R. Howlett, J.C. Richardson, The pathology of APP transgenic mice: a model of Alzheimer's disease or simply overexpression of APP? Histol. Histopathol. 24 (2009) 83—100, https://doi.org/10.14670/hh-24.83.

[4] H.W. Querfurth, J. Jiang, W. Xia, D.J. Selkoe, Enhancer function and novel DNA binding protein activity in the near upstream βAPP gene promoter.pdf, Gene 232 (1999) 125–141.

[5] A. Villa, J. Santiago, B. Belandia, A. Pascual, A response unit in the first exon of the β-amyloid precursor protein gene containing thyroid hormone receptor and Sp1 binding sites mediates negative regulation by 3, 5, 3′-triiodothyronine, Mol. Endocrinol. 18 (2017) 863–873, https://doi.org/10.1210/me.2003-0260.

[6] S. Yoshikaia, Y. Sakakia, Positive and negative regulatory elements for the expression of the Alzheimer' s disease amyloid precursor-encoding gene in mouse, Gene 112 (1992) 189–195.

[7] I. Surgucheva, A. Surguchov, Expression of caveolin in trabecular meshwork cells and its possible implication in pathogenesis of primary open angle glaucoma, Mol. Vis. 17 (2011) 2878–2888.

[8] H. Gu, X. Wei, A.D. Monnot, C. V Fontanilla, M. Behl, M.R. Farlow, W. Zheng, Y. Du, Lead exposure increases levels of β-amyloid in the brain and CSF and inhibits LRP1 expression in APP transgenic mice, Neurosci. Lett. 490 (2011) 16–20, https://doi.org/10.1016/j.neulet.2010.12.017.

[9] A.M. Masoud, S.W. Bihaqi, J.T. Machan, N.H. Zawia, W.E. Renehan, Early-life exposure to lead (Pb) alters the expression of microRNA that target proteins associated with Alzheimer' s disease, J. Alzheimer's Dis. 51 (2016) 1257–1264, https://doi.org/10.3233/JAD-151018.

[10] F.A. Rabito, C. Shorter, L.E. White, Lead levels among children who live in public housing, Epidemiology 14 (2003) 263–268, https://doi.org/10.1097/01.EDE.0000060458.28457.E2.

[11] S. Bolisetty, R. Mezzenga, Amyloid-carbon hybrid membranes for universal water purification, Nat. Nanotechnol. 11 (2016) 365–371, https://doi.org/10.1038/nnano.2015.310.

[12] K.M. Bakulski, L.S. Rozek, D.C. Dolinoy, H.L. Paulson, H. Hu, Alzheimer's disease and environmental exposure to lead: the epidemiologic evidence and potential role of epigenetics, Curr. Alzheimer Res. 9 (2013) 563–573, https://doi.org/10.1016/j.micinf.2011.07.011.Innate.

[13] A. Surguchov, F.N. Emamzadeh, A.A. Surguchev, Amyloidosis and Longevity: A Lesson from Plants, Biology (Basel) vol. 8, (2019), https://doi.org/10.3390/biology8020043.

[14] N.H.Z.M. Riyaz Basha, Wei Wei, Saleh A. Bakheet, Nathalie Benitez, Hasan K. Siddiqi, Yuan-Wen Ge, Debomoy K. Lahiri, The fetal basis of amyloidogenesis: exposure to lead and latent overexpression of amyloid precursor protein and β-amyloid in the aging brain, J. Neurosci. 25 (2005) 823–829, https://doi.org/10.1523/JNEUROSCI.4335-04.2005.

[15] R. Basha, M. Murali, H.K. Siddiqi, K. Ghosal, O.K. Siddiqi, H.A. Lashuel, Y. Ge, D.K. Lahiri, N.H. Zawia, Lead (Pb) exposure and its effect on APP proteolysis and Aβ aggregation, FASEB J. 19 (2005) 2083–2084, https://doi.org/10.1096/fj.05-4375fje.

[16] J. Wu, R. Basha, B. Brock, D.P. Cox, F. Cardozo-pelaez, C.A. Mcpherson, J. Harry, D.C. Rice, B. Maloney, D. Chen, D.K. Lahiri, N.H. Zawia, Alzheimer's disease (AD)-like pathology in aged monkeys after infantile exposure to environmental metal lead (Pb): evidence for a developmental origin and environmental link for AD, J. Neurosci. 28 (2008) 3–9, https://doi.org/10.1523/JNEUROSCI.4405-07.2008.

[17] J.Y. Koh, H.N. Kim, J.J. Hwang, Y.H. Kim, S.E. Park, Lysosomal dysfunction in proteinopathic neurodegenerative disorders: possible therapeutic roles of cAMP and zinc, Mol. Brain 12 (2019) 1, https://doi.org/10.1186/s13041-019-0439-2.

[18] M. Razmiafshari, J. Kao, A. Avignon, N.H. Zawia, NMR identification of heavy metal-binding sites in a synthetic zinc finger peptide: toxicological implications for the interactions of xenobiotic metals with zinc finger proteins, Toxicol. Appl. Pharmacol. 172 (2001) 1–10, https://doi.org/10.1006/taap.2001.9132.

[19] R. Basha, W. Wei, M. Brydie, M. Razmiafshari, N.H. Zawia, Lead-induced developmental perturbations in hippocampal Sp1 DNA-binding are prevented by zinc supplementation: in vivo evidence for Pb and Zn competition, Int. J. Dev. Neurosci. 21 (2003) 1–12, https://doi.org/10.1016/S0736-5748(02)00137-5.

[20] D.S. Atkins, R. Basha, N.H. Zawia, Intracellular signaling pathways involved in mediating the effects of lead on the transcription factor Sp1, Int. J. Dev. Neurosci. 21 (2003) 235–244, https://doi.org/10.1016/S0736-5748(03)00067-4.

[21] L.M. Hellman, M.G. Fried, Electrophoretic mobility shift assay (EMSA) for detecting protein–nucleic acid interactions, Nat. Protoc. 2 (2007) 1849, https://doi.org/10.1038/nprot.2007.249.Electrophoretic.

[22] D.J.G.A. Schmitz, DNAase footprinting a simple method for the detection of protein-DNA binding specificity, Nucleic Acids Res. 5 (1978) 2381–2390.

[23] T.L. Young-pearse, J. Bai, R. Chang, J.B. Zheng, J.J. Loturco, D.J. Selkoe, A critical function for β-amyloid precursor protein in neuronal migration revealed by in utero RNA interference, J. Neurosci. 27 (2007) 14459–14469, https://doi.org/10.1523/JNEUROSCI.4701-07.2007.

[24] R.G. Perez, H. Zheng, L.H.T. Van Der Ploeg, E.H. Koo, The β-amyloid precursor protein of Alzheimer's disease enhances neuron viability and modulates neuronal polarity, J. Neurosci. 17 (1997) 9407–9414.

[25] D.H. Small, V. Nurcombe, R.D. Moir, H. Clarris, A heparin-binding domain in the amyloid protein precursor of Alzheimer's disease is involved in the regulation of neurite outgrowth, J. Neurosci. 14 (2014) 2117–2127.

[26] T.L. Young-Pearse, J. Bai, R. Chang, J.B. Zheng, J.J. LoTurco, D.J. Selkoe, A critical function for -amyloid precursor protein in neuronal migration revealed by in utero RNA interference, J. Neurosci. 27 (2007) 14459–14469, https://doi.org/10.1523/JNEUROSCI.4701-07.2007.

[27] S.L. Sabo, A.F. Ikin, J.D. Buxbaum, P. Greengard, The Alzheimer amyloid precursor protein (APP) and FE65, an APP-binding protein, regulate cell movement, J. Cell Biol. 153 (2001) 1403–1414, https://doi.org/10.1083/jcb.153.7.1403.

[28] M.P. Mattson, Cellular actions of beta-amyloid precursor protein and its soluble and fibrillogenic derivatives, Physiol. Rev. 77 (1997) 1081–1132, https://doi.org/10.1152/physrev.1997.77.4.1081.

[29] A.I. Bush, The metallobiology of Alzheimer's disease, Trends Neurosci. 26 (2003) 207–214, https://doi.org/10.1016/S0166-2236(03)00067-5.

[30] M.R. Basha, The fetal basis of amyloidogenesis: exposure to lead and latent overexpression of amyloid precursor protein and -amyloid in the aging brain, J. Neurosci. 25 (2005) 823–829, https://doi.org/10.1523/JNEUROSCI.4335-04.2005.

[31] J. Michelle, R. Narehood, Lead neurotoxicity: exploring the potential impact of lead substitution in zinc-finger proteins on mental health, Metallomics 8 (2016) 579–588, https://doi.org/10.1039/C5MT00300H.

[32] Y. Li, T. Chen, Y. Wan, S. Xu, Lead exposure in pheochromocytoma cells induces persistent changes in amyloid precursor protein gene methylation patterns, Environ. Toxicol. 27 (2012) 495–502, https://doi.org/10.1002/tox.20666.

[33] N.H. Zawia, R. Sharan, M. Brydie, T. Oyama, T. Crumpton, Sp1 as a target site for

metal-induced perturbations of transcriptional regulation of developmental brain gene expression, Dev. Brain Res. 107 (1998) 291–298.
[34] F. Schwesinger, R. Ros, T. Strunz, D. Anselmetti, H.-J. Guntherodt, A. Honegger, L. Jermutus, L. Tiefenauer, A. Pluckthun, Unbinding forces of single antibody-antigen complexes correlate with their thermal dissociation rates, Proc. Natl. Acad. Sci. 97 (2000) 9972–9977, https://doi.org/10.1073/pnas.97.18.9972.
[35] A. Chilkoti, T. Boland, B.D. Ratner, P.S. Stayton, The relationship between ligand-binding thermodynamics and protein-ligand interaction forces measured by atomic force microscopy, Biophys. J. 69 (1995) 2125–2130, https://doi.org/10.1016/S0006-3495(95)80083-4.
[36] Y.F. Dufrêne, D. Martínez-Martín, I. Medalsy, D. Alsteens, D.J. Müller, Multiparametric imaging of biological systems by force-distance curve–based AFM, Nat. Methods 10 (2013) 847, https://doi.org/10.1038/nmeth.2602.
[37] A.F. Guedes, F.A. Carvalho, I. Malho, N. Lousada, L. Sargento, N.C. Santos, Atomic force microscopy as a tool to evaluate the risk of cardiovascular diseases in patients, Nat. Nanotechnol. 11 (2016) 687–692, https://doi.org/10.1038/nnano.2016.52.
[38] A.V. Krasnoslobodtsev, L.S. Shlyakhtenko, Y.L. Lyubchenko, Probing interactions within the synaptic DNA-SfiI complex by AFM force spectroscopy, J. Mol. Biol. 365 (2007) 1407–1416, https://doi.org/10.1016/j.jmb.2006.10.041.
[39] Z. Lv, R. Roychaudhuri, M.M. Condron, D.B. Teplow, Y.L. Lyubchenko, Mechanism of amyloid β-protein dimerization determined using single-molecule AFM force spectroscopy, Sci. Rep. 3 (2013) 2880, https://doi.org/10.1038/srep02880.
[40] N. Grabe, AliBaba2: context specific identification of transcription factor binding sites, Silico Biol. 2 (2002) S1–S15.
[41] A.C. Kim, S. Lim, Y.K. Kim, Metal ion effects on Aβ and tau aggregation, Int. J. Mol. Sci. 19 (2018) 1–15, https://doi.org/10.3390/ijms19010128.
[42] M. Peydayesh, S. Bolisetty, T. Mohammadi, R. Mezzenga, Assessing the binding performance of amyloid-carbon membranes toward heavy metal ions, Langmuir 35 (2019) 4161–4170, https://doi.org/10.1021/acs.langmuir.8b04234.
[43] F. Gago, E. Marco, R. Garcı, Assessment by molecular dynamics simulations of the structural determinants of DNA-binding specificity for transcription factor Sp1, J. Mol. Biol. 328 (2003) 9–32, https://doi.org/10.1016/S0022-2836(03)00243-2.
[44] C.J. Narayan VA, R.W. Kriwacki, Structures of zinc finger domains from transcription factor Sp1 insights into sequence-specific protein-DNA recognition, J. Biol. Chem. 272 (1997) 7801–7809, https://doi.org/10.1074/jbc.272.12.7801.
[45] X. Du, Y. Li, Y. Xia, S. Ai, J. Liang, P. Sang, X. Ji, Insights into protein–ligand interactions: mechanisms, models, and methods, Int. J. Mol. Sci. 17 (2016) 144, https://doi.org/10.3390/ijms17020144.
[46] M. Valentino, R.M. Fiorini, G. Curatola, M. Governa, Changes of membrane fluidity in erythrocytes of lead-exposed workers, Int. Arch. Occup. Environ. Health 51 (1982) 105–112, https://doi.org/10.1016/0006-291X(77)90223-6.
[47] E. Moeendarbary, A.R. Harris, Cell mechanics: principles, practices, and prospects, Wiley Interdiscip. Rev. Syst. Biol. Med. 6 (2014) 371–388, https://doi.org/10.1002/wsbm.1275.
[48] E. Moeendarbary, L. Valon, M. Fritzsche, A.R. Harris, D.A. Moulding, A.J. Thrasher, E. Stride, L. Mahadevan, G.T. Charras, The cytoplasm of living cells behaves as a poroelastic material, Nat. Mater. 12 (2013) 253, https://doi.org/10.1038/NMAT3517.
[49] T. Müller, C.G. Concannon, M.W. Ward, C.M. Walsh, A.L. Tirniceriu, F. Tribl, D. Kögel, J.H. Prehn, R. Egensperger, Modulation of gene expression and cytoskeletal dynamics by the amyloid precursor protein intracellular domain (AICD), Mol. Biol. Cell 18 (2007) 201–210, https://doi.org/10.1091/mbc.E06.
[50] N.C. Gauthier, M.A. Fardin, P. Roca-Cusachs, M.P. Sheetz, Temporary increase in plasma membrane tension coordinates the activation of exocytosis and contraction during cell spreading, Proc. Natl. Acad. Sci. 108 (2011) 14467–14472, https://doi.org/10.1073/pnas.1105845108.
[51] N.C. Gauthier, T.A. Masters, M.P. Sheetz, Mechanical feedback between membrane tension and dynamics, Trends Cell Biol. 22 (2012) 527–535, https://doi.org/10.1016/j.tcb.2012.07.005.
[52] D. Pesen, J.H. Hoh, Micromechanical architecture of the endothelial cell cortex, Biophys. J. 88 (2005) 670–679, https://doi.org/10.1529/biophysj.104.049965.
[53] P.R. Goode, J. Qiu, E. Palle, W.B. Rossow, A.W. Walker, D.E. Beuschel, W.M. Or, Elastic behavior of cross-linked and bundled actin networks, Science 304 (80-) (2004) 1301–1306, https://doi.org/10.1126/science.1095087.
[54] T. Munder, A. Pfeffer, S. Schreyer, J. Guo, J. Braun, I. Sack, B. Steiner, MR Elastography Detection of Early Viscoelastic Response of the Murine hippocampus to Amyloid β Accumulation and Neuronal Cell Loss Due to Alzheimer's Disease, (2017), https://doi.org/10.1002/jmri.25741.
[55] D.A. Fletcher, R.D. Mullins, Cell mechanics and the cytoskeleton, Nature 463 (2010) 485.
[56] M.P. Mattson, Cellular actions of beta-amyloid precursor protein and its soluble and fibrillogenic derivatives, Physiol. Rev. 77 (1997) 1081–1132, https://doi.org/10.1152/physrev.1997.77.4.1081.
[57] T. Verina, C.A. Rohde, T.R. Guilarte, J. Hopkins, Environmental lead exposure during early life alters granule cell neurogenesis and morphology in the hippocampus of young adult rats, Neuroscience 145 (2007) 1037–1047, https://doi.org/10.1016/j.neuroscience.2006.12.040.
[58] J. Kronlage, C, M. Schäfer-Herte, D. Böning, H. Oberleithner, Fels, Feeling for filaments: quantification of the cortical actin web in live vascular endothelium, Biophys. J 109 (2015) 687–698, https://doi.org/10.1016/j.bpj.2015.06.066.
[59] L. Pujadas, D. Rossi, R. Andrés, C.M. Teixeira, B. Serra-Vidal, A. Parcerisas, R. Maldonado, E. Giralt, N. Carulla, E. Soriano, Reelin delays amyloid-beta fibril formation and rescues cognitive deficits in a model of Alzheimer's disease, Nat. Commun. 5 (2014) ncomms4443, https://doi.org/10.1038/ncomms4443.
[60] Y. Fang, C.Y.Y. Iu, C.N.P. Lui, Y. Zou, C.K.M. Fung, H.W. Li, N. Xi, K.K.L. Yung, K.W.C. Lai, Investigating dynamic structural and mechanical changes of neuroblastoma cells associated with glutamate-mediated neurodegeneration, Sci. Rep. 4 (2014) 7074, https://doi.org/10.1038/srep07074.
[61] E.M. Darling, S. Zauscher, F. Guilak, Viscoelastic properties of zonal articular chondrocytes measured by atomic force microscopy, Osteoarthr. Cartil. 14 (2006) 571–579, https://doi.org/10.1016/j.joca.2005.12.003.
[62] V.A. Narayan, R.W. Kriwacki, J.P. Caradonna, Structures of zinc finger domains from transcription factor Sp1, J. Biol. Chem. 272 (1997) 7801–7809, https://doi.org/10.1021/bi9727646.